9800 *Biochemistry* **2010,** *49,* 9800–9808
DOI: 10.1021/bi101364t

BIOCHEMISTRY
including biophysical chemistry & molecular biology
Article

Effects of pH on the S_3 State of the Oxygen Evolving Complex in Photosystem II Probed by EPR Split Signal Induction[†]

Johannes Sjöholm, Kajsa G. V. Havelius,[‡] Fikret Mamedov, and Stenbjörn Styring*

Molecular Biomimetics, Department of Photochemistry and Molecular Science, Ångström Laboratory, Uppsala University, P.O. Box 523, SE-751 20 Uppsala, Sweden. [‡]*Present address: Department of Physics, Freie Universität Berlin, Arnimallee 14, 14195 Berlin, Germany.*

Received August 24, 2010; Revised Manuscript Received October 6, 2010

ABSTRACT: The electrons extracted from the $CaMn_4$ cluster during water oxidation in photosystem II are transferred to P_{680}^+ via the redox-active tyrosine D1-Tyr161 (Y_Z). Upon Y_Z oxidation a proton moves in a hydrogen bond toward D1-His190 (His_Z). The deprotonation and reprotonation mechanism of Y_Z-OH/Y_Z-O is of key importance for the catalytic turnover of photosystem II. By light illumination at liquid helium temperatures (~5 K) Y_Z can be oxidized to its neutral radical, $Y_Z^\bullet$. This can be followed by the induction of a split EPR signal from $Y_Z^\bullet$ in a magnetic interaction with the $CaMn_4$ cluster, offering a way to probe for Y_Z oxidation in active photosystem II. In the S_3 state, light in the near-infrared region induces the split S_3 EPR signal, $S_2'Y_Z^\bullet$. Here we report on the pH dependence for the induction of $S_2'Y_Z^\bullet$ between pH 4.0 and pH 8.7. At acidic pH the split S_3 EPR signal decreases with the apparent pK_a (pK_{app}) ~ 4.1. This can be correlated to a titration event that disrupts the essential H-bond in the Y_Z-His_Z motif. At alkaline pH, the split S_3 EPR signal decreases with the pK_{app} ~ 7.5. The analysis of this pH dependence is complicated by the presence of an alkaline-induced split EPR signal (pK_{app} ~ 8.3) promoted by a change in the redox potential of Y_Z. Our results allow dissection of the proton-coupled electron transfer reactions in the S_3 state and provide further evidence that the radical involved in the split EPR signals is indeed $Y_Z^\bullet$.

The first step in the photosynthetic oxygen evolution is light excitation of the primary electron donor chlorophylls, P_{680}, in photosystem II (PSII).[1] An electron is transferred through the acceptor side of PSII via the first electron acceptor, Pheo, and the quinone acceptors Q_A and Q_B. After two electrons have reached Q_B, it dissociates into the thylakoid membrane (*1*, *2*). Electrons to reduce P_{680}^+ are ultimately derived from water on the donor side of PSII. The catalytic site for water oxidation is the $CaMn_4$ cluster, and the mechanism for water oxidation is generally described in a four-step oxidation process ($S_n \rightarrow S_{n+1}$, n = 0−4), known as the S-cycle (*3*). By assuming a sequential and alternate extraction of electrons and protons throughout the cycle, the process can also be described in eight discrete steps (*4*). This "extended S-cycle" highlights the importance of controlled electron and proton movements on the donor side of PSII to keep the redox potential of the $CaMn_4$ cluster in balance to facilitate dioxygen formation. After accumulating four oxidizing equivalents (forming the transient S_4 state in the OEC), two water molecules are oxidized, O_2 is released, and the S_0 state is regenerated.

The electrons extracted from the $CaMn_4$ cluster are transferred to P_{680}^+ via the tyrosine residue Y_Z. When Y_Z is oxidized, it forms a neutral radical by a coupled deprotonation of the phenolic proton (*5*). The proton moves in a hydrogen bond to the nearby base His_Z (*6*, *7*). Y_Z is rereduced by the $CaMn_4$ cluster within microseconds to milliseconds at room temperature (*8*, *9*). By lowering the temperature, light-induced Y_Z oxidation is still possible but the S-state transitions freeze out completely below ~80 K (*10*). Illumination of a PSII sample at liquid helium temperatures has made it possible to observe the otherwise transient $Y_Z^\bullet$ on spectroscopic time scales in intact PSII preparations (*11*). In EPR spectroscopy the line shape of the organic radical from $Y_Z^\bullet$ will be broadened by a magnetic interaction with the closely lying $CaMn_4$ cluster. This results in a series of EPR signals, denoted the split EPR signals, reflecting the magnetic interaction between $Y_Z^\bullet$ and the $CaMn_4$ cluster. Since the shape of the signals are dependent on the spin state of the $CaMn_4$ cluster, the split EPR signals offer good spectroscopic probes to the different S-states of the OEC (*12*).

The split EPR signals from the S_0 and S_1 states can be induced by visible light at liquid helium temperatures through P_{680}^+-driven charge separation (*13*, *14*). The electron transfer from Q_A to Q_B is blocked at this temperature, creating the charge pair $Y_Z^\bullet Q_A^-$ that recombines with $t_{1/2}$ ~ 3 min at 5 K (*15*). The split

[†]The Swedish Research Council, the Swedish Energy Agency, the Knut and Alice Wallenberg Foundation, The EU program SOLAR-H2 (EU Contract 212508), and the Nordic Energy Research Program 06-Hydr-C13 are gratefully acknowledged for financial support.

*Corresponding author: phone, +46 18 471 6580; fax, +46 471 6844; e-mail, stenbjorn.styring@fotomol.uu.se.

[1]Abbreviations: AMPSO, 3-[(1,1-dimethyl-2 hydroxyethyl)amino]-2-hydroxypropanesulfonic acid; $CaMn_4$ cluster, the catalytic center consisting of four Mn ions and one Ca ion; Car, carotenoid; Chl, chlorophyll; Cytb_{559}, cytochrome b_{559}; D1 and D2, the core protein subunits in PSII; DAD, 3,6-diaminodurene; DMSO, dimethyl sulfoxide; EPR, electron paramagnetic resonance; HEPES, *N*-(2-hydroxyethyl)piperazine-*N*′-2-ethanesulfonic acid; His_Z, histidine 190 on the D1 protein that participates in hydrogen bonding to Y_Z; MES, 2-(*N*-morpholino)-ethanesulfonic acid; NIR, near-infrared; OEC, oxygen evolving complex consisting of the $CaMn_4$ cluster and surrounding amino acid ligands; P_{680}, primary electron donor chlorophylls in PSII; P*p*BQ, phenyl-*p*-benzoquinone; PSII, photosystem II; Pheo, pheophytin acceptor in PSII; Q_A and Q_B, primary and secondary plastoquinone acceptors of PSII; S states, intermediates in the cyclic turnover of the OEC; Y_D, tyrosine 161 on the D2 protein; Y_Z, tyrosine 161 on the D1 protein.

 Published on Web 10/06/2010

EPR signals from the S_2 and S_3 states can also be induced by near-infrared (NIR) illumination (*16*, *17*). P_{680} does not absorb light in this spectral region (740−900 nm), and the NIR-induced split signals are believed to originate from excitation of the $CaMn_4$ cluster itself. A NIR sensitivity of the $CaMn_4$ cluster was first observed as a low- to high-spin transition in the S_2 state (*18*, *19*), and the effect has been attributed to a charge transfer among the Mn ions (*18*) or a spin-state change of Mn(III) in the cluster (*19*−*21*). It has now been shown that the split S_3 EPR signal can be induced by light also in the visible spectral range (415−730 nm) and not only by NIR light as previously thought (*22*). Recently, it was also suggested that the same mechanism is responsible for the formation of the split S_3 EPR signal independent of the wavelength of the inducing light (*23*), and it was questioned whether Mn(IV) excitation could be excluded. The formation of the split S_3 EPR signal is proposed to stem from the excitation of the $CaMn_4$ cluster to a potential high enough to oxidize the nearby residue Y_Z (*16*, *24*). This will lead to a modified S_2 state, denoted S_2', which interacts with $Y_Z^{\bullet}$, giving rise to the split S_3 EPR signal. The S_2' state is likely to be a proton-deficient configuration of the S_2 state (*25*, *26*). This state is rather similar to a state induced by exposure of the S_3 state to high pH, a treatment that also gives rise to a split EPR signal (*27*).

Independent of inducing light, formation of $Y_Z^{\bullet}$ observed as a split EPR signal will require deprotonation of the phenol proton even at liquid helium temperatures. Since the low temperature severely restricts proton movements, this implies that electron transfer can only occur when Y_Z is frozen in a configuration that promotes proton transfer at low temperature. This configuration probably involves a strong hydrogen bond to the N_ε of His_Z in the Y_Z−His_Z hydrogen bond motif, supported by a well-set H-bond network in the OEC (*11*). The pH dependence of the split EPR signal formation can provide information on the limitations of the Y_Z−His_Z motif. This has previously been assessed in the S_0 and S_1 states of the OEC by following the induction of the split EPR signals as a function of pH (*28*−*30*). In the present study we expand these investigations to include the pH dependence of the split EPR signal induced from the S_3 state.

MATERIALS AND METHODS

PSII Membrane Preparation. PSII-enriched membranes (BBY type) were prepared from hydroponically grown spinach (*Spinacia oleracea*) as described previously (*31*, *32*). The preparation was kept at −80 °C in a buffer containing 25 mM MES−NaOH (pH 6.3), 15 mM NaCl, 3 mM $MgCl_2$, and 400 mM sucrose. The steady-state oxygen evolution from the BBY membrane preparation was ∼350 μmol of O_2 (mg of Chl)$^{-1}$ h^{-1}. Oxygen evolution was determined with a Clark-type electrode at ∼20 μg of Chl/mL measured under saturating light at 20 °C in a buffer with 25 mM MES−NaOH (pH 6.3), 10 mM NaCl, 5 mM $MgCl_2$, 5 mM $CaCl_2$, and 400 mM sucrose using 0.5 mM P*p*BQ as an electron acceptor. Chl concentrations were determined according to Arnon (*33*).

Synchronization of the OEC and S-State Advancement. The PSII membranes were washed two times and diluted to ∼2.5 mg of Chl/mL in a low buffering medium (2 mM MES −NaOH (pH 6.3), 10 mM NaCl, 5 mM $MgCl_2$, 5 mM $CaCl_2$, and 300 mM sucrose) before being put into calibrated EPR tubes. All samples were exposed to room light for 5 min to fully oxidize Y_D and then dark adapted for 30 min. The $CaMn_4$ cluster was synchronized in the dark-stable S_1 state by giving one preflash and then dark adapted for 15 min at 20 °C (*10*, *34*). P*p*BQ was added to a final concentration of 1 mM (from a 50 mM stock solution in DMSO) after the preflash procedure. The S_3 state was achieved by giving two saturating turnover laser flashes to the EPR sample at 0 °C. Flashes were provided by a Nd:YAG laser (Spectra Physics, USA) at 5 Hz frequency (532 nm, 850 mJ/pulse). The typical S-state composition after two flashes was ∼65% S_3 and 35% S_2 as calculated from the yield of the S_2 state multiline EPR signal (*12*).

pH Jump. After the turnover flashes the pH of the samples was rapidly changed (< 5 s) by adding a buffering medium at 150 mM (for the corresponding pH range pH 3.3−4.25, glutamic acid−NaOH; pH 4.6−6.6, MES−NaOH; pH 6.8−7.8, HEPES−NaOH; pH 8.0−8.7, glycylglycine−NaOH; pH 8.8−9.5, AMPSO) to achieve a final concentration of 20 mM (*29*, *35*). The samples were frozen in a dry ice/ethanol bath within 10 s after the pH adjustment.

EPR Spectroscopy. Continuous-wave EPR measurements were performed in the dark with a Bruker ELEXSYS E500 spectrometer using a SuperX EPR049 microwave bridge. Low-temperature experiments were carried out with a Bruker SHQ 4122 cavity equipped with an Oxford Instruments cryostat and ITC 503 temperature controller using liquid helium as coolant. The split S_3 EPR signal was induced at 5 K by continuous NIR illumination (830 nm) directly into the cavity. The light was provided by a LQC830-135E continuous laser diode (Newport, USA). The light intensity at the position of the cavity window was 67 W/m^2. After illumination, the EPR samples were incubated in complete darkness at 5 K in the cavity. Signal processing and quantification were carried out with the Bruker Xepr software. Spectrometer settings are given in the figure legends.

Sample Evaluation and EPR Signal Analysis. Despite fast sample handling, the $CaMn_4$ cluster might sustain pH-induced damage in a fraction of the PSII centers leading to partial loss of oxygen evolution (*29*, *30*, *35*). This damage is pH and time dependent, occurring faster at extreme pH (*27*, *35*). To control this, the remaining oxygen evolution after the EPR measurements was measured in each individual sample at pH 6.3. The pH in the samples were brought back by dilution to ca. 20 μg of Chl/mL in the 25 mM MES−NaOH buffer to equilibrate at pH 6.3. The oxygen evolution measurement was conducted within 20 s after the EPR sample was thawed; 90% of the samples retained more than 70% of the maximum O_2 evolution (on average the correction factor was 0.85). Samples with less than 50% of their activity remaining were removed from the analysis. In samples where the activity was lowered, the data points (EPR signal amplitudes) were corrected to full activity (*29*, *30*). In this way irreversible split EPR signal loss, due to pH-induced damage of PSII or the OEC, could be removed from the analysis. In addition, the final pH and the Chl concentration of each EPR sample were measured. The EPR signal amplitude was normalized to the found Chl concentration, which could vary somewhat between the samples due to the elaborate sample preparation protocol.

The difference EPR spectra shown in Figure 1B and in Figure 2 are obtained by subtraction of the spectrum recorded in dark from the spectrum recorded 1 min after the NIR illumination was stopped. This was done in order to minimize any temperature effects on the signal intensity due to our long (30 min) illumination procedure. Although cooled to 5 K in the cavity, the sample will heat up slightly during the 830 nm irradiation. In cases where spectra recorded in the dark are reported, a small sample-independent contribution from the EPR cavity was always removed.

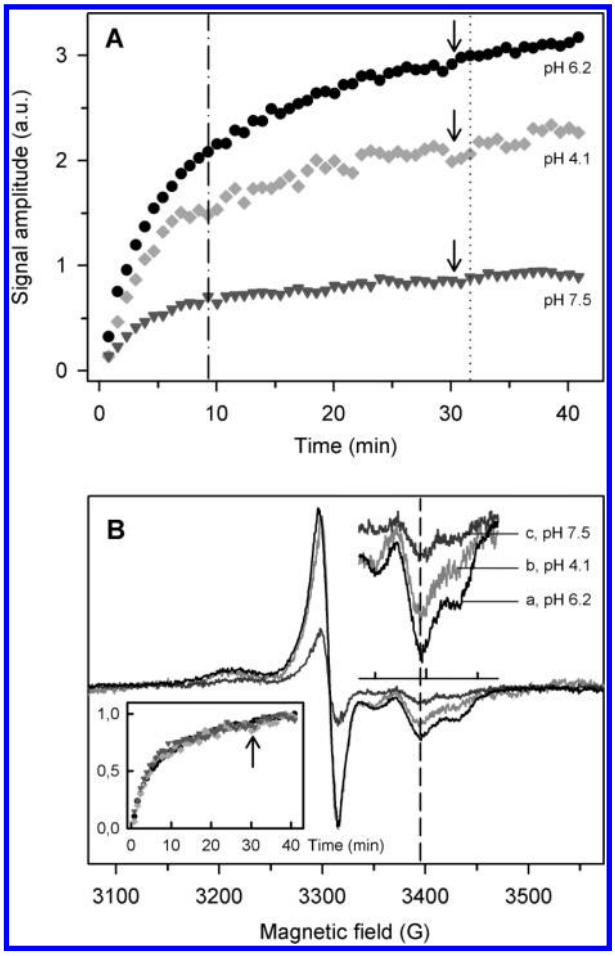

FIGURE 1: Induction of the split S_3 EPR signal at 5 K by illumination with 830 nm light of PSII centers in the S_3 state. (A) The induction of the split S_3 EPR signal at 5 K was followed for 30 min during continuous NIR illumination and during 10 min after light was turned off (arrows) in samples at pH 6.2 (black circles), pH 4.1 (light gray diamonds), and pH 7.5 (dark gray triangles). Each data point represents the signal intensity at 3395 G (indicated by a dashed line in panel B) measured in a field-swept spectrum. The time point at which the signal amplitude was measured for analysis of the pH dependence of the split S_3 EPR signal presented in Figure 3 is indicated by a dash-dotted line. (B) EPR spectra of the split S_3 EPR signal at pH 6.2 (a), pH 4.1 (b), and pH 7.5 (c). The difference spectra shown are obtained by subtracting the spectrum before illumination from the spectrum 1 min after illumination is stopped. The time point at which the spectra are taken is indicated by a dotted line in panel A. The inset shows the induction of the split S_3 EPR signal at pH 6.2 (black circles), pH 4.1 (light gray diamonds), and pH 7.5 (dark gray triangles) after normalizing the maximal amplitudes to facilitate comparison of the induction kinetics at different pHs. EPR parameters: temperature 5 K, microwave frequency 9.279 GHz, microwave power 25 mW, and modulation amplitude 10 G.

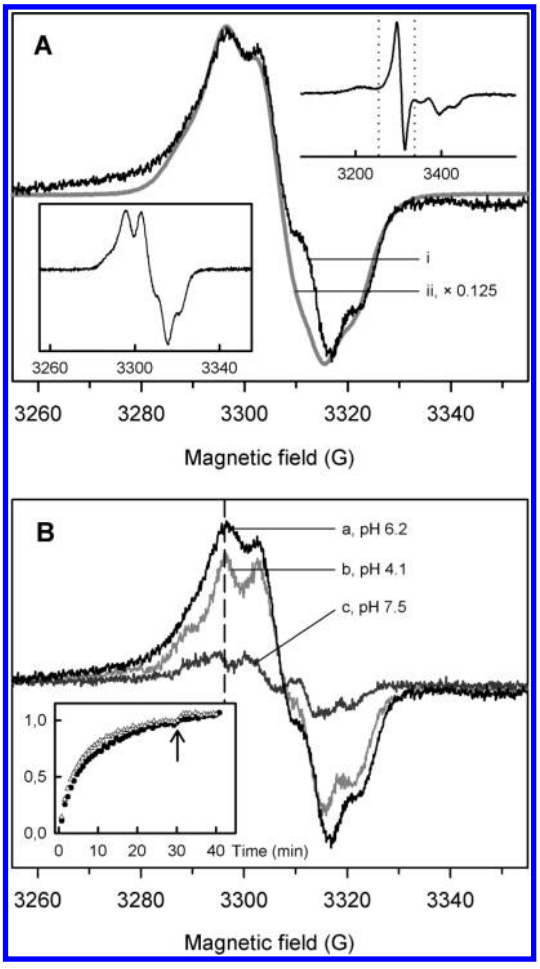

FIGURE 2: Resolved radical EPR spectra in the $g \sim 2$ region of the split S_3 EPR signal, induced by 830 nm illumination at 5 K. (A) Spectrum i shows the difference EPR spectrum induced by 30 min illumination at 5 K at pH 6.2. Spectrum ii shows the EPR spectrum of $Y_D^\bullet$ before illumination, measured in the same sample under the same EPR conditions (note the difference in scale). The upper right inset shows the entire light-induced spectrum recorded as in Figure 1, and the dotted lines indicate the field region of the radical spectra in Figure 2 in relation to the split S_3 EPR signal. The lower left inset shows the spectrum of $Y_D^\bullet$ recorded under nonsaturating conditions. (B) EPR spectra induced by NIR illumination at 5 K in the radical region at pH 6.2 (a), pH 4.1 (b), and 7.5 (c). The inset shows the induction kinetics of the EPR signal in the radical region (white triangles) by 830 nm illumination at 5 K of a sample at pH 6.2. The signal was followed for 30 min in light and subsequently 10 min in dark. Each data point represents the signal intensity at 3296 G (indicated by a dashed line) measured in a field-swept spectrum. The induction of the split EPR signal (pH 6.2) measured as in Figure 1 (black circles) is shown for comparison. The maximal amplitudes have been normalized. EPR parameters: temperature 5 K, microwave frequency 9.279 GHz, microwave power 1 mW, and modulation amplitude 3.2 G. The spectrum in the upper right inset in panel A was measured as in Figure 1. The inset spectrum of $Y_D^\bullet$ was measured at 10 K, microwave frequency 9.279 GHz, microwave power 0.5 μW, and modulation amplitude 3.2 G.

RESULTS

NIR illumination at liquid helium temperatures of PSII membranes poised in the S_3 state results in the formation of a metalloradical EPR signal, the split S_3 EPR signal (*16*, *22*). Compared to the split signals originating from the S_1 (*13*, *14*), S_2 (*36*), and S_0 (*14*) states, the mechanism behind the formation of the split S_3 EPR signal by illumination with NIR light is different. It is thought to involve excitation of one of the Mn ions in the $CaMn_4$ cluster as opposed to P_{680}-driven charge separation. The excited Mn ion oxidizes the nearby Y_Z giving rise to a broadened radical EPR signal. Although referred to as the split S_3 EPR signal, it is believed that it arises from a magnetic interaction between $Y_Z^\bullet$ and an oxidation state of the $CaMn_4$ cluster formally similar to the S_2 state, denoted $S_2'Y_Z^\bullet$ (*16*, *25*, *26*).

Here, we have investigated the pH dependence of the NIR-induced split S_3 EPR signal. By continuous 830 nm illumination at 5 K of a sample at normal pH (pH 6.2), the maximum split S_3 EPR signal intensity was reached after ca. 30 min. Quantification, based on the parallel decay of the Q_AFe^{2+} signal (when Q_A^- is present from the start), indicates that this accounts for up to ~74% of the PSII centers that were in the S_3 state in a two-flash

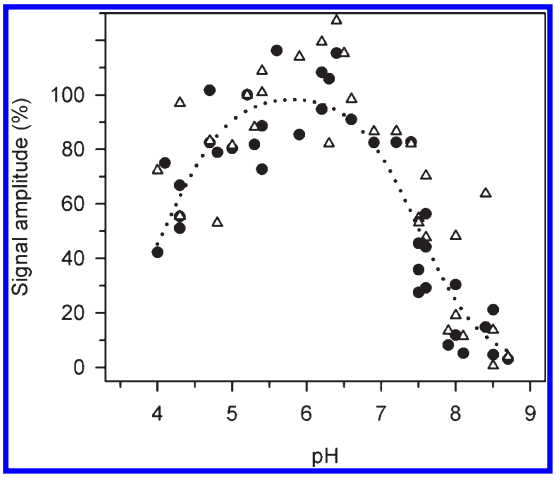

FIGURE 3: pH dependence of the split S_3 EPR signal induced by 830 nm illumination for 9 min at 5 K. Black circles show the normalized amplitudes measured on the high-field trough at 3395 G (indicated by a dashed line in Figure 1B) of the split S_3 EPR signal. White triangles show the normalized amplitudes measured on the peak at 3296 G (indicated by a dashed line in Figure 2B) of the $g \sim 2.0043$ radical component of the split S_3 EPR signal. The measured amplitudes are corrected for the fraction of irreversibly damaged centers (see Materials and Methods). The dotted line shows the pH-dependent behavior of the split S_3 EPR signal fitted with the combination of the two pK_{app}s (4.1 and 7.5) obtained from the half-inhibition of the signal amplitude.

sample (for details see ref *23*). The pH dependence was addressed in PSII samples exposed to two flashes (predominantly in the S_3 state) by changing the pH with the addition of a strong molar buffer. The buffer addition was made only after the sample had reached the S_3 state, thereby avoiding any influence of pH effects on the transitions from $S_1 \rightarrow S_2 \rightarrow S_3$.

Induction of the Split S_3 EPR Signal. Figure 1A shows the induction of the split S_3 EPR signal by continuous NIR illumination at pH 6.2 (black circles), pH 4.1 (light gray diamonds), and pH 7.5 (dark gray triangles). The amplitude of the signal was measured at 3395 G in a field-swept spectrum (indicated by a dashed line in panel B). After 30 min the illumination was stopped, indicated by an arrow in Figure 1A. When the samples were kept in dark at 5 K in the cavity, the split S_3 EPR signal intensity was stable. The stability of the EPR signal stems from the lack of recombination partner (Q_A^-) when the sample is illuminated with NIR light. This is different from the split S_3 EPR signal generated with visible light that decays partly over time by recombination with Q_A^- (*22*). By observing the signal amplitude after 30 min illumination, it is clear that the maximum yield of the split S_3 EPR signal is dependent on pH, decreasing both at low and at high pH. It is important to note that the kinetics for the induction is the same independent of pH. This is shown in the lower inset in Figure 1B, where the induction traces have been normalized to the maximum amplitude at the respective pH.

Figure 1B shows the spectra of the split S_3 EPR signal at the time point indicated with a dotted line in Figure 1A for the respective pH (pH 6.2, pH 4.1, and pH 7.5). The spectra presented are difference spectra obtained by subtraction of the dark trace from the trace following the 5 K illumination (see Materials and Methods). At normal pH (Figure 1B, black spectrum) the split S_3 EPR signal is composed of a large double trough at 3395 G, a smaller trough at 3350 G, a weak low-field peak at 3210 G, and a derivative-shaped signal centered at $g \sim 2$. The overall splitting of the broadened radical is 140−210 G, with the peak to the large central trough separated by ca. 185 G. The detailed structure of the derivate shape at $g \sim 2$ is not clearly defined in Figure 1B due to the high modulation amplitude (10 G). This inner radical component is instead more thoroughly analyzed in Figure 2 where lower modulation amplitude was utilized (see below).

The spectral shape of the split S_3 EPR signal was not affected by a change to either low or high pH (Figure 1B, light gray and dark gray spectrum, respectively), but the signal intensity was clearly decreasing. At pH 4.1 the signal intensity, measured on the trough at 3395 G (Figure 1B, dashed line), was 79% compared to the intensity at pH 6.2. At pH 7.5 the signal intensity decreased to 29%.

Resolving the Split S_3 EPR Signal at $g \sim 2$. Figure 2A shows the $g \sim 2$ derivative signal induced at normal pH (pH 6.2) and the spectrum of $Y_D^\bullet$, both recorded at 3.2 G modulation amplitude. Unlike visible illumination at 5 K, the 830 nm illumination does not induce any Chl/Car radical (*15*, *22*). This makes the spectral features of the pure split S_3 EPR signal in the $g \sim 2$ region easy to derive by illumination-minus-dark subtraction. The split S_3 radical shows a resolved tyrosine-like structure that is 20 G wide with $g \sim 2.0043$, similar to the reported values for $Y_Z^\bullet$ and $Y_D^\bullet$ (19 G, $g \sim 2.0046$) (*37*). The spectrum of $Y_D^\bullet$ in Figure 2A (gray spectrum, note the scale) is not well resolved at this microwave power and recording temperature. At 1 mW microwave power and 5 K the spectrum of $Y_D^\bullet$ is subjected to rapid passage effects due to its slow relaxation (*38*), distorting the tyrosine fine structure. The lower left inset in Figure 2A shows the spectrum of $Y_D^\bullet$ recorded at low microwave power (0.5 μW) for comparison.

In Figure 2B the central radical part of the split S_3 EPR signal is shown at pH 6.2, pH 4.1, and pH 7.5. The signal intensity decreased at both low and high pH with 75% and 18% remaining relative to the amplitude at pH 6.2, respectively. The induction of the central radical component was followed during 30 min continuous NIR illumination of a sample at pH 6.2. The inset in Figure 2B (white triangles) shows the change in the normalized amplitude measured at 3296 G (dashed line, Figure 2B). The inset also shows the induction of the broad split S_3 EPR signal component (black circles) measured at 3395 G (dashed line, Figure 1B). The induction kinetics of the central radical component is almost identical to the induction of the broad split S_3 EPR signal component.

pH Dependence of the Split S_3 EPR Signal. By measuring the amplitude of the split S_3 EPR signal induced at 5 K, the pH dependence of the signal could be resolved between pH 4.0 and pH 8.7. The pH-independent induction kinetics (Figure 1) of the split S_3 EPR signal allowed us to analyze the EPR signal amplitude without having to reach saturation with the NIR illumination. Figure 3 (black circles) shows the normalized signal amplitudes of the broad split S_3 component measured at 3395 G (dashed line, Figure 1B) after 9 min of NIR illumination (the time point is indicated with a dash-dotted line in Figure 1A). In the same figure (Figure 3, white triangles), the normalized amplitudes of the $g \sim 2$ radical component measured at 3296 G (dashed line, Figure 2B) are plotted against the pH. We conclude that the split S_3 EPR signal shows the same pH dependence when analyzed at the split trough or at the $g \sim 2$ radical.

The pH treatment has the potential of causing damage to the OEC and the $CaMn_4$ cluster, especially at extreme pHs (*27*, *35*). Irreversibly damaged centers will not form the split S_3 EPR signal upon illumination. The integrity of the $CaMn_4$ was analyzed by measuring the steady-state oxygen evolution after reversing the pH of the EPR sample to pH ~6.3. The rates were largely

unaffected by the pH treatment (see Materials and Methods). In cases where the activity was lowered, the split EPR signal amplitude was corrected to full activity. In Figure 3, the signal amplitudes have been compensated for the lost PSII centers. This compensation eliminates a pH-dependent decrease of the split signal originating from centers where the $CaMn_4$ cluster was destroyed (i.e., PSII centers with no O_2 evolution). The observed pH dependence is by this only a consequence of protonation/deprotonation-induced inhibition of the split EPR signal formation.

The mean split S_3 EPR signal amplitudes that were measured between pH 5.4 and pH 6.4 is set as 100% in Figure 3. The amplitude decreases at both low and high pH. The half-inhibition of the signal, i.e., where the signal has lost 50% of its maximal amplitude, occurs at pH 4.1 and 7.5 on the low- and high-pH side, respectively. These pH values are assumed to correspond to the pH at which the protonation probability is 0.5. We assign these pH values to the apparent pK_a (pK_{app}) values for the decrease of the split S_3 EPR signal. The dotted line in Figure 3 is a fit of the split S_3 EPR signal amplitudes between pH 4.0 and pH 8.7 using the two pK_{app} values 4.1 and 7.5.

A High-pH-Induced Split Signal Is Present in the Dark. It was previously reported that when the pH of a sample poised in the S_3 state is changed from normal to alkaline in the dark, the EPR spectrum is changed (*27*). A new resonance appears around $g \sim 2$, with a shoulder and trough separated by ~100 G around the radical signal of $Y_D^\bullet$. The signal was suggested to arise from a $S_2Y_Z^\bullet$ state (hereafter denoted the $S_2''Y_Z^\bullet$ state) of the OEC, formed by a high-pH-induced decrease of the $Y_Z^\bullet/Y_Z$ redox potential shifting the $S_3Y_Z \leftrightharpoons S_2Y_Z^\bullet$ equilibrium to the right (*27*). A similar appearance of a broadened radical EPR spectrum at alkaline pH was observed also in this study. Figure 4A shows EPR spectra recorded prior to illumination at increasing pH (spectra a−d). At pH 7.6 (Figure 4A, spectrum a) the large background signal of $Y_D^\bullet$ totally dominated the spectrum. When gradually increasing the pH, a peak at 3245 G and a trough at 3370 G appeared (observed together with the signal from $Y_D^\bullet$). At pH 8.7 (Figure 4A, spectrum d) the EPR spectrum clearly resembled the EPR spectra previously reported by Geijer et al. (*27*).

The induction of the high-pH-induced split EPR signal was followed by measuring the change in signal amplitude between 3245 and 3370 G, indicated by dashed lines in Figure 4A. In Figure 4B the signal amplitude is plotted against the pH (white triangles) between pH 4.7 and pH 8.7. Above pH ~7.5 there is a sharp increase in the signal intensity, reaching maximum amplitude at pH 8.7. The pH dependence of the split S_3 EPR signal on the high-pH side is shown for comparison. The inset in Figure 4B shows the high-pH-induced split EPR signal ($S_2''Y_Z^\bullet$, black spectrum) and the NIR-minus-dark signal (gray spectrum) induced in the same sample at pH 8.4. It is clear that the NIR-induced split signal ($S_2'Y_Z^\bullet$) is not present at this pH. The half-inhibition of the signal, corresponding to the pK_{app} for a single protonable group, was estimated to ~8.3. The titration curve in Figure 4B (dashed line) was fitted with pK_{app} 8.3 with the assumption that the signal has reached its maximum at pH 8.7.

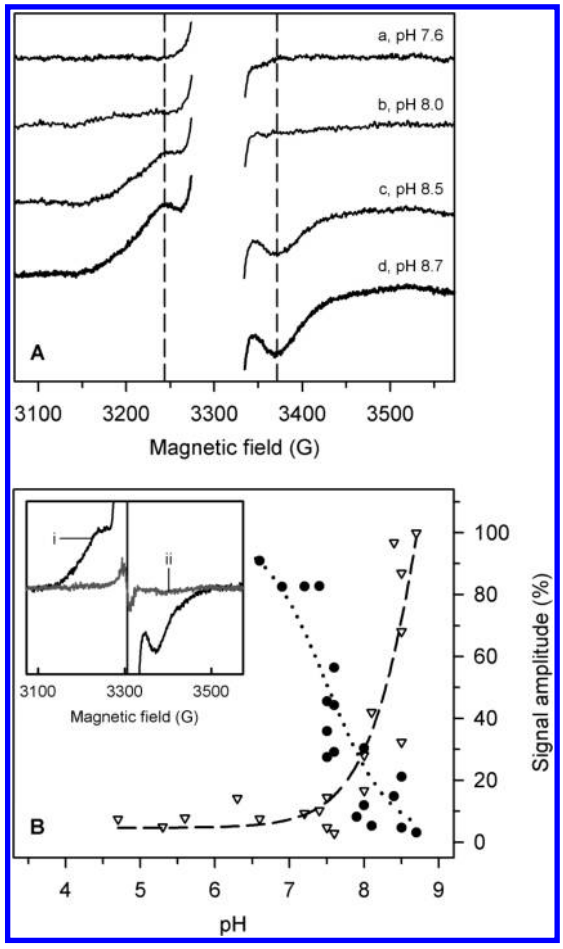

FIGURE 4: Induction of the high-pH-induced split EPR signal ($S_2''Y_Z^\bullet$) of samples in the S_3 state. (A) Normalized EPR spectra measured at 5 K of samples at pH 7.6 (a), pH 8.0 (b), pH 8.5 (c), and pH 8.7 (d). The large signal from $Y_D^\bullet$ appearing at $g \sim 2$ (3307 G) has been omitted for clarity. (B) Titration of the high-pH-induced split EPR signal (white triangles). The signal amplitude was measured between 3245 and 3370 G (indicated by dashed lines in panel A). The fitting of the data points (dashed line) was made for one protonable group with pK_{app} 8.3. The high-pH side of the titration of the split S_3 EPR signal (black circles, dotted line) is shown as comparison (from Figure 3). The inset shows the EPR spectra of a sample at pH 8.4 recorded before illumination (i) and the NIR-induced signal (illumination minus dark) recorded after 9 min illumination (ii). EPR parameters: temperature 5 K, microwave frequency 9.279 GHz, microwave power 25 mW, and modulation amplitude 10 G.

DISCUSSION

Here we report on the pH dependence of the split S_3 EPR signal between pH 4.0 and pH 8.7. A sample poised in the S_3 state is illuminated with 830 nm light at 5 K. The resulting split EPR resonance is thought to originate from the spin−spin interaction between a modified S_2 state (denoted S_2') and the neutral radical $Y_Z^\bullet$. The S_2' state is created by a "backward" electron transfer from Y_Z upon NIR excitation of the $CaMn_4$ cluster at 5 K (Scheme 1a). The modification refers to the lack of one proton in that state, since the proton lost during the catalytic $S_2 \rightarrow S_3$ transition cannot be replaced at 5 K. The exact mechanism behind the NIR sensitivity of the $CaMn_4$ cluster is debated and will not be addressed further here.

It was initially thought that the split S_3 EPR signal could be induced only by illumination in the NIR spectral region. However, it is now known that the signal can be induced by monochromic light from 415 to 900 nm (*22*), and strong evidence supports a single mechanism for the induction in the whole spectral range (*23*). Here we have used NIR illumination for the induction of the split S_3 EPR signal for two reasons. In a sample exposed to two flashes, ca. 35% of the PSII centers will still be in the S_2 state. Since no S_2 state EPR signal induced by NIR light overlaps with the split S_3 EPR signal, centers in the S_2 state will not complicate the analysis. In addition, NIR illumination does

Scheme 1: pH-Induced Changes Affecting the Oxidation of Y_Z and the S_3 State at Normal (a), Low (b), or High (c) pH

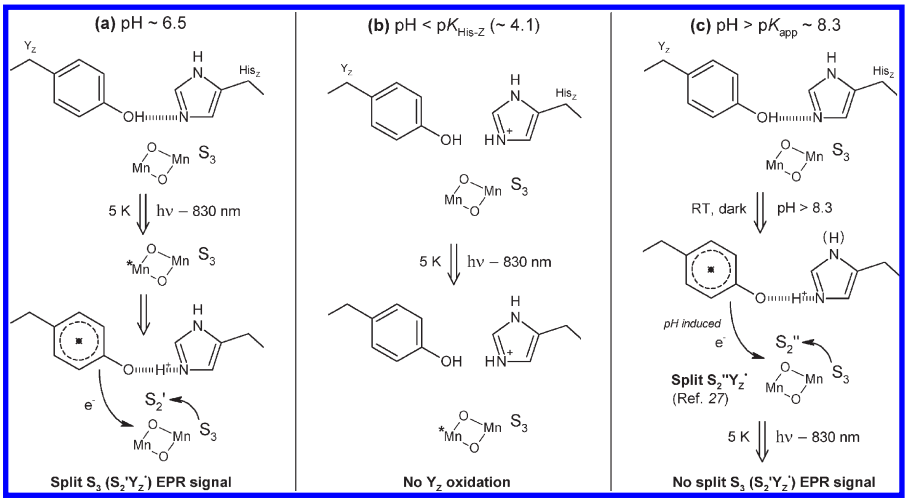

not result in oxidation of the secondary electron donors Cyt b_{559} or Car/Chl (*22*). This is useful since the ~20 G wide radical signal will not suffer from contribution of oxidized Car or Chl. This is not the case for the split EPR signals when they are induced with visible light (*15*, *29*, *30*).

The maximal amplitude of the split S_3 EPR signal is reached after ca. 30 min 830 nm illumination, and the signal is stable in the dark at 5 K after the illumination is stopped. The stability of the signal is a consequence of its origin since the normal recombination partner Q_A^- is not formed through charge separation by the NIR induction (*22*). It is also clear that the signal does not decay by recombination with the $CaMn_4$ cluster at 5 K under the time period followed in the experiment. Under low modulation the $g \sim 2$ radical component of the split S_3 EPR signal is well resolved and shows a tyrosine-like signature with $g \sim 2.0043$ and a width of 20 G. This is not the case for the signal of $Y_D^\bullet$ recorded under the same conditions (as shown in Figure 2A). At 1 mW and 5 K the spin−lattice relaxation rate of $Y_D^\bullet$ is too slow as compared to the modulation frequency used, and the spectrum is distorted due to the rapid passage effect (*38*). The increased resolution of the hyperfine structure of the $g \sim 2$ radical component indicates that it is faster relaxing than $Y_D^\bullet$. Presumably, the residue resides in a close position to the $CaMn_4$ cluster, which enhances its relaxation. Both the shape of the radical signal and its fast relaxation lead us to assign the 20 G wide component of the split S_3 EPR signal to $Y_Z^\bullet$.

The spectral components of the split S_3 EPR signal, including both the 185 G splitting and the $g \sim 2$ derivative, have been observed previously (*16*, *22*, *39*). They were suggested to arise from the spin $^1/_2$ of the $Y_Z^\bullet$ radical interacting with the $CaMn_4$ cluster in a spin $^7/_2$ configuration (*40*). From the decay-associated spectrum of the split S_3 EPR signal (induced by visible light at 5 K) it was concluded that the different parts of the spectrum cannot be separated by microwave power saturation (*15*). As shown here, the induction kinetics is identical for both signal parts. Furthermore, their pH dependence is the same (which is not the case for the corresponding components of the split S_0 EPR signal (*30*)). We therefore consider the composite of the 185 G splitting and the $g \sim 2$ derivative to represent the true feature of split S_3 EPR signal, and in the following we therefore address their pH dependence as arising from PSII centers in the same structural configuration. In contrast, we find it premature to attempt simulation of the EPR spectra given the lacking knowledge about the magnetic and spin properties of the $CaMn_4$ cluster in the S_2' state.

Table 1: pH-Dependent Induction of Split EPR Signals and Function of the S-State Transitions in the Low-pH Region

split signal	pK_a	S-state transition	pK_a
$S_1Y_Z^\bullet$	4.7−4.9[b]	$S_1 \rightarrow S_2$	pH independent[d]
$S_2'Y_Z^\bullet$	4.1[a]	$S_2 \rightarrow S_3$	3.8−4.0[d]
$S_0Y_Z^\bullet$	4.7−4.8[c]	$S_0 \rightarrow S_1$	4.7[d]

[a] pK_{app} reported in this work. [b] From refs *28* and *29*. [c] From refs *28* and *30*. [d] From refs *48* and *49*.

Low pH: Protonation of the Y_Z−His_Z Hydrogen Bond Motif. At low pH, the split S_3 EPR signal induced at 5 K decreases with p$K_{app} \sim 4.1$. This is similar (but not identical; see below) to the decrease of the split S_0 (~4.7−4.8) and split S_1 (~4.7−4.9) EPR signals induced at 5 K (Table 1) (*28*−*30*). Thus, all split EPR signals investigated so far decrease with an pK_a of 4.1−4.9 (4.6 ± 0.3). This similarity leads us to propose that the reason for the decrease is the same in all S-states. Consequently, the decrease of the split S_3 EPR signal is explained in the same way as the decrease of the split EPR signals induced from the S_0 (*30*) and S_1 (*29*) states. When lowering the pH, the essential Y_Z−His_Z hydrogen bond motif is disrupted. The most straightforward explanation is a direct titration of His_Z. In this situation no other proton acceptor is available at this temperature. Therefore, oxidation of Y_Z is not possible (Scheme 1b). This is observed as a loss of split EPR signal formation.

Although not dissected for the separate S-states, similar pK_as (~4.5−5.3) are found for the decrease of the nanosecond kinetics in the reduction of P_{680}^+ by Y_Z, measured at ambient temperature (*41*−*45*). The nanosecond kinetics is thought to represent an electron transfer not rate limited by a subsequent proton transfer and reflects oxidation of Y_Z coupled to a proton that shifts in a well-set hydrogen bond between Y_Z and the nearby His_Z (*46*, *47*). Thus, both the nanosecond kinetics at ambient temperature and the split EPR signal formation at 5 K decrease concertedly with similar pK_as, presumably by protonation of the Y_Z−His_Z motif. It seems that this is not S-state dependent. Breaking the hydrogen bond involving Y_Z-OH always slows down or inhibits Y_Z oxidation (depending on temperature).

The mechanism for the induction of the split S_3 EPR signal is different from the split EPR signals induced from the S_0 and S_1 states. In the S_3 state, Y_Z is oxidized via electron transfer back to the $CaMn_4$ cluster (Scheme 1a). Since the experiment is carried out

at 5 K, reprotonation of the OEC cannot take place. Therefore, the end state, $S_2'Y_Z^\bullet$, will represent an OEC with a physical structure of the $CaMn_4$ cluster, including the number of associated protons, comparable to the S_3 configuration but with an oxidation state equivalent to that found in S_2. Interestingly, the pK_{app} for the backward formation of the $S_2'Y_Z^\bullet$ state is similar to the pK_a for the inhibition of the forward transition between $S_2 \rightarrow S_3$ at ambient temperature that was found to be ~4.0 when measured by EPR (*48*) and ~3.6 when measured by FTIR (*49*) (Table 1). The forward reaction at 20 °C and the backward reaction at 5 K can be described by eq 1.

$$S_2Y_Z^\bullet(20\ °C) \rightarrow S_3Y_Z \rightarrow (5\ K,\ 830\ nm) \rightarrow S_2'Y_Z^\bullet \qquad (1)$$

It seems that the pK_as of both reactions in eq 1 are considerably lower than for the induction of $S_0Y_Z^\bullet$ (~4.7−4.8) and $S_1Y_Z^\bullet$ (~4.7−4.9) (Table 1) (*28*−*30*). The lower pK_{app} for the induction of $S_2'Y_Z^\bullet$ probably reflects the overall charge situation in the OEC in the S_3 state. The proton release during water oxidation is on average 1:0:1:2 for the $S_0 \rightarrow S_1 \rightarrow S_2 \rightarrow S_3 \rightarrow S_4$ transitions (*50*−*53*). The release pattern is consistent with electrochromic band shift measurements showing the net charge change 0:+1:0:−1 for the corresponding transitions (*54*, *55*). In the $S_0 \rightarrow S_1$ transition one electron and one proton are released from the $CaMn_4$ cluster without a change in the net charge of the OEC. In the $S_1 \rightarrow S_2$ transition there is no proton release coupled to the oxidation, and one positive charge is accumulated on the $CaMn_4$ cluster. $Y_Z^\bullet$ formation in the S_2 state is suggested to be followed by a charge-compensating proton release from the OEC before the electron transfer, and subsequent transition to the S_3 state occurs (*4*). The proton release conserves the single positive charge from the S_2 state, leaving the S_3 state in a positive, high-potential state. This charge will most likely cause a downshift in the pK_a(s) of a nearby amino acid(s). It could directly affect the pK_a of the Y_Z−His_Z motif or alter its pK_a via an interconnected H-bond network.

Even though the induction of the split S_3 EPR signal occurs by oxidation of Y_Z via electron transfer back to the $CaMn_4$ cluster, it is a proton-coupled reaction steered by a pK_{app} of ~4.1. At 5 K proton movements are severely restricted, and Y_Z must be involved in a very well defined hydrogen bond to be oxidized. Its oxidation cannot be dependent on any large-scale proton rearrangements. The pK_{app} ~ 4.1 can therefore be assigned to the Y_Z−His_Z motif and the low pK_{app} to the extra charge on the $CaMn_4$ cluster in the S_3 state.

High pH: pH-Induced Y_Z Oxidation Hinders Split EPR Signal Formation. By increasing the pH, the split S_3 EPR signal decreases with pK_{app} ~ 7.5 when induced by NIR illumination at 5 K. With the exception of the $S_3 \rightarrow (S_4) \rightarrow S_0$ transition there is no significant decrease in any of the S-state transitions at alkaline pH (below pH ~9) (*48*, *49*). This indicates that at ambient temperature there are no pH constraints on the transitions between $S_0 \rightarrow S_1 \rightarrow S_2 \rightarrow S_3$ above pH ~6. It also indicates that Y_Z oxidation is possible at high pH at ambient temperature. The induction of the split S_1 EPR signal with visible light at 5 K is pH independent above pH ~6, which signifies that Y_Z oxidation is possible at high pH even at this temperature (*29*). The induction of the split S_0 EPR signal decreases with pK_{app} ~ 7.9. However, the decrease observed at pH above 7.7 was suggested to be caused by a pH-induced change of the $CaMn_4$ cluster, affecting the magnetic interaction to $Y_Z^\bullet$, and not to be significantly affected by an inhibition of Y_Z oxidation by high pH (*30*). Thus, it seems that Y_Z oxidation is not inhibited by high pH neither at ambient temperature nor at 5 K.

The observed decrease of the split S_3 EPR signal at high pH is accordingly likely to be due to reasons other than inhibition of Y_Z oxidation and is in fact easily explainable at least at pH above ~7.5. At pH >7.5, a 125 G wide split EPR signal is formed already in the dark, i.e., without any inducing illumination. The signal has previously been characterized and suggested to arise from a proton-deficient $S_2Y_Z^\bullet$ state (*27*). It is thought to originate from electron transfer from Y_Z back to the S_3 state of the $CaMn_4$ cluster, reducing it to a proton-deficient S_2 state, denoted S_2''. This was explained by the pH-dependent redox potential of the $Y_Z^\bullet/Y_Z$ couple which was suggested to be lowered by the alkaline pH to a potential below that of the S_3/S_2 redox couple. The induction of the dark-induced split EPR signal overlaps with the decrease of the NIR-induced split S_3 EPR signal. It makes sense that the presence of $S_2''Y_Z^\bullet$ (formed already before the sample is illuminated) prevents the induction of the split S_3 EPR signal by NIR illumination at 5 K. If Y_Z is already oxidized at pH ~7.5−8.7, it can obviously not be oxidized by NIR-induced excitation of the $CaMn_4$ cluster (Scheme 1c). Consequently, the amplitude of the NIR-induced split S_3 EPR signal will be significantly decreased even if there is no major inhibition of Y_Z oxidation in the S_3 state due to the high pH.

Interestingly, even though both the split S_3 EPR signal and the high-pH-induced split EPR signal arise from an interaction between $Y_Z^\bullet$ and a modified S_2 state, the signal shapes are significantly different (compare Figures 1B and 4A). At the moment we find it most reasonable to explain this by the different induction temperatures. The split S_3 EPR signal is induced by illumination at 5 K while the high-pH-induced EPR signal is induced by a change of pH in the dark before the sample is frozen. The induction of the modified S_2'' state occurs at ambient temperature which will allow larger protein rearrangements. It is likely that even small structural differences in the $CaMn_4$ cluster will give rise to different interaction signals. The high-pH-induced split EPR signal ($S_2''Y_Z^\bullet$) is actually more similar in shape to another $S_2 \rightarrow S_3$ transition intermediate, with a peak and trough separated by 116 G (*36*). The latter signal is induced from a sample in the S_2 state by illumination at higher temperature (77−190 K) and can be trapped by a rapid cooling to 10 K.

The pH-dependent induction of the $S_2''Y_Z^\bullet$ state in the dark was fitted with a pK_{app} ~ 8.3 (Figure 4B) and is similar to what was reported by Geijer et al. (~8.5) (*27*). However, we note that the signal does not level off before pH 8.7, the upper pH limit in this investigation, introducing an uncertainty in the determined pK_{app}. The decrease of the split S_3 EPR signal at pHs above 6.5 (pK_{app} ~ 7.5) is not perfectly concomitant with the increase of the $S_2''Y_Z^\bullet$ state (pK_{app} ~ 8.3) as indicated by the 0.8 pH unit difference of the pK_{app}s. The reason for this discrepancy is not clear, but the initial decrease of the split S_3 EPR signal at mild alkaline pH (< 7.5) must be caused by something other than the dark oxidation of Y_Z that occurs above pH ~7.5. In the following we address the apparent discrepancy.

In Geijer et al. (see Figure 8 in ref *27*) two possible scenarios were presented to explain the change in the relative midpoint potentials between $Y_Z^\bullet/Y_Z$ and S_3/S_2. Either (i) the redox potential of the $Y_Z^\bullet/Y_Z$ couple is pH dependent, decreasing at alkaline pH, while the S_3/S_2 couple has a pH-independent potential or (ii) both the potential of $Y_Z^\bullet/Y_Z$ and S_3/S_2 decrease concomitantly at increasing pH. In both cases, at pH above ~8.3−8.5 the potential of $Y_Z^\bullet/Y_Z$ would become lower than for the S_3/S_2 couple inducing the $S_2''Y_Z^\bullet$ state. In (ii) a pH-dependent decrease in the redox potential of the S_3/S_2 couple could reflect changes in the $CaMn_4$

complex that lead to for example a drop in efficiency of Y_Z oxidation by the NIR illumination at mild alkaline pH, thereby lowering the yield of the split S_3 EPR signal. Our present study does not further clarify this situation. The reason is that oxidation of Y_Z by NIR light in the S_3 state probably involves excitation of one of the Mn ions in the $CaMn_4$ cluster, and very little is known about the redox potentials for this excited Mn ion. Even less is known about its pH dependence. This makes it premature to speculate about a pH-dependent NIR sensitivity of Mn and potential structural or magnetic reasons for this.

Instead, we refer to our earlier studies of the S_0 state to provide a possible explanation for the discrepancy we observe (*30*). In the S_0 state, the initial decrease of the split S_0 EPR signal between pH 6.6 and pH 7.7 was not explained by a pH-induced change of the $CaMn_4$ cluster, suggested to occur above pH∼7.7 (see above). Instead, the slight decrease at mild alkaline pH was suggested to be caused by a changed hydrogen bond network around Y_Z, presumably by p*K* changes in the local environment of the Y_Z−His_Z motif. A destabilization of the hydrogen bond network would not necessarily affect the oxidation of Y_Z at ambient temperature, as observed by pH-independent nanosecond kinetics at high pH (*41*, *43*), but could retard the efficiency of Y_Z oxidation at 5 K. It is not unlikely that the same effect is seen at mild alkaline pH in the S_3 state. In this case a destabilization of the same hydrogen bond network would decrease the yield of the split S_3 EPR signal even before Y_Z was dark oxidized by the S_3 state due to the high pH (> 7.5). As a result a 0.8 pH unit difference is observed in the pK_{app}s.

In conclusion, the pH dependences of the split EPR signals investigated so far, $S_1Y_Z^{\bullet}$, $S_2'Y_Z^{\bullet}$, and $S_0Y_Z^{\bullet}$, have similar pH dependencies in the low-pH region (pK_a ∼ 4.1−4.9 (*28*−*30*)). In all cases the decrease is assigned to the disruption of the essential H-bond in the Y_Z−His_Z motif (*29*, *30*), and it can be concluded that this is independent of whether the split EPR signal formation occurs via "forward" or "backward" electron transfer. At pH above ∼7.5 the formation of the split S_3 EPR signal is hindered by the induction of another split EPR signal, $S_2''Y_Z^{\bullet}$. This state is induced by a change in the redox potential of Y_Z (*27*) and also implies that there is no major inhibition of Y_Z oxidation at high-pH values. Interestingly, such a change in redox potential of Y_Z is not affecting the formation of the split EPR signal induced from the S_1 state at high pH (*29*). This might reflect the importance of the charge-compensating proton release taking place in the $S_2 \rightarrow S_3$ transition. Furthermore, as shown previously the split S_3 EPR signal does not decay by recombination with the $CaMn_4$ cluster (*22*), and this is shown here to be pH independent. The stability of the split S_3 EPR signal is interesting and deserves further attention.

ACKNOWLEDGMENT

The authors thank Dr. Felix Ho for helpful discussions.

REFERENCES

1. Barber, J. (2003) Photosystem II: The engine of life. *Q. Rev. Biophys. 36*, 71–89.
2. Renger, G. (2008) Functional pattern of photosystem II, in Primary processes of photosynthesis—Part 2 (Renger, G., Ed.) pp 237−290, RSC Publishing, Cambridge, U.K.
3. McEvoy, J. P., and Brudvig, G. W. (2006) Water-splitting chemistry of photosystem II. *Chem. Rev. 106*, 4455–4483.
4. Dau, H., and Haumann, M. (2007) Eight steps preceding O-O bond formation in oxygenic photosynthesis—A basic reaction cycle of the photosystem II manganese complex. *Biochim. Biophys. Acta 1767*, 472–483.
5. Tommos, C., Tang, X. S., Warncke, K., Hoganson, C. W., Styring, S., McCracken, J., Diner, B. A., and Babcock, G. T. (1995) Spin-density distribution, conformation, and hydrogen-bonding of the redox-active tyrosine Y_Z in photosystem II from multiple electron magnetic-resonance spectroscopies: Implications for photosynthetic oxygen evolution. *J. Am. Chem. Soc. 117*, 10325–10335.
6. Mamedov, F., Sayre, R. T., and Styring, S. (1998) Involvement of histidine 190 on the D1 protein in electron/proton transfer reactions on the donor side of photosystem II. *Biochemistry 37*, 14245–14256.
7. Hays, A. M. A., Vassiliev, I. R., Golbeck, J. H., and Debus, R. J. (1998) Role of D1-His190 in proton-coupled electron transfer reactions in photosystem II: A chemical complementation study. *Biochemistry 37*, 11352–11365.
8. Rappaport, F., Blanchard-Desce, M., and Lavergne, J. (1994) Kinetics of electron transfer and electrochromic change during the redox transitions of the photosynthetic oxygen-evolving complex. *Biochim. Biophys. Acta 1184*, 178–192.
9. Razeghifard, M. R., Klughammer, C., and Pace, R. J. (1997) Electron paramagnetic resonance kinetic studies of the S states in spinach thylakoids. *Biochemistry 36*, 86–92.
10. Styring, S., and Rutherford, A. W. (1988) Deactivation kinetics and temperature-dependence of the S-state transitions in the oxygen-evolving system of photosystem II measured by EPR spectroscopy. *Biochim. Biophys. Acta 933*, 378–387.
11. Havelius, K. G. V., Sjöholm, J., Ho, F., Mamedov, F., and Styring, S. (2010) Metalloradical EPR signals from the $Y_Z^{\bullet}$S-state intermediates in photosystem II. *Appl. Magn. Reson. 37*, 151–176.
12. Han, G., Ho, F. M., Havelius, K. G. V., Morvaridi, S. F., Mamedov, F., and Styring, S. (2008) Direct quantification of the four individual S states in photosystem II using EPR spectroscopy. *Biochim. Biophys. Acta 1777*, 496–503.
13. Nugent, J. H., Muhiuddin, I. P., and Evans, M. C. (2002) Electron transfer from the water oxidizing complex at cryogenic temperatures: The S_1 to S_2 step. *Biochemistry 41*, 4117–4126.
14. Zhang, C., and Styring, S. (2003) Formation of split electron paramagnetic resonance signals in photosystem II suggests that $tyrosine_Z$ can be photooxidized at 5 K in the S_0 and S_1 states of the oxygen-evolving complex. *Biochemistry 42*, 8066–8076.
15. Havelius, K. G. V., Su, J. H., Feyziyev, Y., Mamedov, F., and Styring, S. (2006) Spectral resolution of the split EPR signals induced by illumination at 5 K from the S_1, S_3, and S_0 states in photosystem II. *Biochemistry 45*, 9279–9290.
16. Ioannidis, N., and Petrouleas, V. (2000) Electron paramagnetic resonance signals from the S_3 state of the oxygen-evolving complex. A broadened radical signal induced by low-temperature near-infrared light illumination. *Biochemistry 39*, 5246–5254.
17. Koulougliotis, D., Shen, J. R., Ioannidis, N., and Petrouleas, V. (2003) Near-IR irradiation of the S_2 state of the water oxidizing complex of photosystem II at liquid helium temperatures produces the metalloradical intermediate attributed to $S_1Y_Z^{\bullet}$. *Biochemistry 42*, 3045–3053.
18. Boussac, A., Girerd, J. J., and Rutherford, A. W. (1996) Conversion of the spin state of the manganese complex in photosystem II induced by near-infrared light. *Biochemistry 35*, 6984–6989.
19. Boussac, A., Kuhl, H., Un, S., Rogner, M., and Rutherford, A. W. (1998) Effect of near-infrared light on the S_2-state of the manganese complex of photosystem II from *Synechococcus elongatus*. *Biochemistry 37*, 8995–9000.
20. Baxter, R., Krausz, E., Wydrzynski, T., and Pace, R. J. (1999) Identification of the near-infrared absorption band from the Mn cluster of photosystem II. *J. Am. Chem. Soc. 121*, 9451–9452.
21. Horner, O., Riviere, E., Blondin, G., Un, S., Rutherford, A. W., Girerd, J. J., and Boussac, A. (1998) SQUID magnetization study of the infrared-induced spin transition in the S_2 state of photosystem II: Spin value associated with the $g = 4.1$ EPR signal. *J. Am. Chem. Soc. 120*, 7924–7928.
22. Su, J. H., Havelius, K. G. V., Ho, F. M., Han, G., Mamedov, F., and Styring, S. (2007) Formation spectra of the EPR split signals from the S_0, S_1, and S_3 states in photosystem II induced by monochromatic light at 5 K. *Biochemistry 46*, 10703–10712.
23. Havelius, K. G. V., Ho, F., Su, J.-H., Han, G., Mamedov, F., Styring, S. (2010) The formation of the split EPR signal from the S_3 state of photosystem II does not involve primary charge separation, *Biochim. Biophys. Acta* (doi:10.1016/j.bbabio.2010.1009.1006).
24. Ioannidis, N., Nugent, J. H., and Petrouleas, V. (2002) Intermediates of the S_3 state of the oxygen-evolving complex of photosystem II. *Biochemistry 41*, 9589–9600.
25. Nugent, J. H., Turconi, S., and Evans, M. C. (1997) EPR investigation of water oxidizing photosystem II: detection of new EPR signals at cryogenic temperatures. *Biochemistry 36*, 7086–7096.

26. Ioannidis, N., and Petrouleas, V. (2002) Decay products of the S_3 state of the oxygen-evolving complex of photosystem II at cryogenic temperatures. Pathways to the formation of the $S = 7/2$ S_2 state configuration. *Biochemistry 41*, 9580–9588.
27. Geijer, P., Morvaridi, F., and Styring, S. (2001) The S_3 state of the oxygen-evolving complex in photosystem II is converted to the $S_2Y_Z^{\bullet}$ state at alkaline pH. *Biochemistry 40*, 10881–10891.
28. Zhang, C. (2006) Interaction between tyrosine$_Z$ and substrate water in active photosystem II. *Biochim. Biophys. Acta 1757*, 781–786.
29. Havelius, K. G., and Styring, S. (2007) pH dependent competition between Y_Z and Y_D in photosystem II probed by illumination at 5 K. *Biochemistry 46*, 7865–7874.
30. Sjöholm, J., Havelius, K. G. V., Mamedov, F., and Styring, S. (2009) The S_0 state of the water oxidizing complex in photosystem II: pH dependence of the EPR split signal induction and mechanistic implications. *Biochemistry 48*, 9393–9404.
31. Berthold, D. A., Babcock, G. T., and Yocum, C. F. (1981) A highly resolved, oxygen-evolving photosystem II preparation from spinach thylakoid membranes. *FEBS Lett. 134*, 231–234.
32. Völker, M., Ono, T., Inoue, Y., and Renger, G. (1985) Effect of trypsin on PS II particles: Correlation between Hill-activity, Mn-abundance and peptide pattern. *Biochim. Biophys. Acta 806*, 25–34.
33. Arnon, D. I. (1949) Copper enzymes in isolated chloroplasts. Polyphenoloxidase in *Beta vulgaris*. *Plant Physiol. 24*, 1–15.
34. Styring, S., and Rutherford, A. W. (1987) In the oxygen-evolving complex of photosystem II the S_0 state is oxidized to the S_1 state by D^+ (Signal-II$_{slow}$). *Biochemistry 26*, 2401–2405.
35. Geijer, P., Deak, Z., and Styring, S. (2000) Proton equilibria in the manganese cluster of photosystem II control the intensities of the S_0 and S_2 state $g \sim 2$ electron paramagnetic resonance signals. *Biochemistry 39*, 6763–6772.
36. Ioannidis, N., Zahariou, G., and Petrouleas, V. (2006) Trapping of the S_2 to S_3 state intermediate of the oxygen-evolving complex of photosystem II. *Biochemistry 45*, 6252–6259.
37. Miller, A.-F., and Brudvig, G. W. (1991) A guide to electron paramagnetic resonance spectroscopy of photosystem II membranes. *Biochim. Biophys. Acta 1056*, 1–18.
38. Styring, S. A., and Rutherford, A. W. (1988) The microwave-power saturation of signal II$_{slow}$ varies with the redox state of the oxygen-evolving complex in photosystem-II. *Biochemistry 27*, 4915–4923.
39. Sugiura, M., Rappaport, F., Brettel, K., Noguchi, T., Rutherford, A. W., and Boussac, A. (2004) Site-directed mutagenesis of *Thermosynechococcus elongatus* photosystem II: the O_2-evolving enzyme lacking the redox-active tyrosine D. *Biochemistry 43*, 13549–13563.
40. Sanakis, Y., Ioannidis, N., Sioros, G., and Petrouleas, V. (2001) A novel $S = 7/2$ configuration of the Mn cluster of photosystem II. *J. Am. Chem. Soc. 123*, 10766–10767.
41. Christen, G., Seeliger, A., and Renger, G. (1999) $P680^{+\bullet}$ reduction kinetics and redox transition probability of the water oxidizing complex as a function of pH and H/D isotope exchange in spinach thylakoids. *Biochemistry 38*, 6082–6092.
42. Ahlbrink, R., Haumann, M., Cherepanov, D., Bogershausen, O., Mulkidjanian, A., and Junge, W. (1998) Function of tyrosine Z in water oxidation by photosystem II: Electrostatical promotor instead of hydrogen abstractor. *Biochemistry 37*, 1131–1142.
43. Schlodder, E., and Meyer, B. (1987) pH-dependence of oxygen evolution and reduction kinetics of photooxidized chlorophyll-a_{II} (P-680) in photosystem II particles from *Synechococcus* sp. *Biochim. Biophys. Acta 890*, 23–31.
44. Meyer, B., Schlodder, E., Dekker, J. P., and Witt, H. T. (1989) O_2 evolution and Chl-a_{II}^+ ($P\text{-}680^+$) nanosecond reduction kinetics in single flashes as a function of pH. *Biochim. Biophys. Acta 974*, 36–43.
45. Kühn, P., Pieper, J., Kaminskaya, O., Eckert, H. J., Lechner, R. E., Shuvalov, V., and Renger, G. (2005) Reaction pattern of photosystem II: Oxidative water cleavage and protein flexibility. *Photosynth. Res. 84*, 317–323.
46. Schilstra, M. J., Rappaport, F., Nugent, J. H. A., Barnett, C. J., and Klug, D. R. (1998) Proton/hydrogen transfer affects the S state-dependent microsecond phases of $P680^+$ reduction during water splitting. *Biochemistry 37*, 3974–3981.
47. Christen, G., and Renger, G. (1999) The role of hydrogen bonds for the multiphasic $P680^{+\bullet}$ reduction by Y_Z in photosystem II with intact oxygen evolution capacity. Analysis of kinetic H/D isotope exchange effects. *Biochemistry 38*, 2068–2077.
48. Bernat, G., Morvaridi, F., Feyziyev, Y., and Styring, S. (2002) pH dependence of the four individual transitions in the catalytic S-cycle during photosynthetic oxygen evolution. *Biochemistry 41*, 5830–5843.
49. Suzuki, H., Sugiura, M., and Noguchi, T. (2005) pH dependence of the flash-induced S-state transitions in the oxygen-evolving center of photosystem II from *Thermosynechoccocus elongatus* as revealed by Fourier transform infrared spectroscopy. *Biochemistry 44*, 1708–1718.
50. Fowler, C. F. (1977) Proton evolution from photosystem II: Stoichometry and mechanistic considerations. *Biochim. Biophys. Acta 462*, 414–421.
51. Förster, F., and Junge, W. (1985) Stoichiometry and kinetics of proton release upon photosynthetic water oxidation. *Photochem. Photobiol. 41*, 183–190.
52. Schlodder, E., and Witt, H. T. (1999) Stoichiometry and proton release from the catalytic center in photosynthetic water oxidation. *J. Biol. Chem. 274*, 30387–30392.
53. Suzuki, H., Sugiura, M., and Noguchi, T. (2009) Monitoring proton release during photosynthetic water oxidation in photosystem II by means of isotope-edited infrared spectroscopy. *J. Am. Chem. Soc. 131*, 7849–7857.
54. Saygin, Ö., and Witt, H. T. (1985) Evidence for the electrochromic identification of the change of charges in the four oxidation steps of photoinduced water cleavage in photosynthesis. *FEBS Lett. 187*, 224–226.
55. Kretschmann, H., Schlodder, E., and Witt, H. T. (1996) Net charge oscillation and proton release during water oxidation in photosynthesis. An electrochromic band shift study at pH 5.5−7.0. *Biochim. Biophys. Acta 1274*, 1–8.